Appl. Phys. B 77, 673–680 (2003)
DOI: 10.1007/s00340-003-1324-2

Applied Physics B
Lasers and Optics

Z.-M. SHENG[1,✉]
J. ZHANG[1]
D. UMSTADTER[2]

Plasma density gratings induced by intersecting laser pulses in underdense plasmas

[1] Laboratory of Optical Physics, Institute of Physics, Chinese Academy of Sciences, Beijing 100080, P.R. China
[2] Center for Ultrafast Optical Science, University of Michigan, Ann Arbor, MI 48109, USA

Received: 25 February 2003/Revised version: 30 July 2003
Published online: 29 October 2003 • **© Springer-Verlag 2003**

ABSTRACT Electron and ion density gratings induced by two intersecting ultrashort laser pulses at intensities of 10^{16} W/cm^2 or lower are investigated. The ponderomotive force generated by the inhomogeneous intensity distribution in the intersecting region of the interfering pulses produces deep electron and ion density modulations at a wavelength less than a laser wavelength in vacuum. Dependence of the density modulation on the plasma densities, temperatures, and the ion mass, as well as the laser pulse parameters are studied analytically and by particle-in-cell simulations. It is found that the density peaks of such gratings can be a few times that of the initial plasma density and last as long as a few picoseconds. It is also demonstrated that the scattering of signal pulses by such a bulk density grating results in high-harmonic generation. The density gratings may be incorporated into ion-ripple lasers [K.R. Chen and J.M. Dawson, Phys. Rev. Lett. **68**, 29 (1992)] to generate ultrashort X-ray pulses of a few angstroms by using electron beams at only a few tens of MeV only.

PACS 52.35.Mw; 42.65.Ky; 52.25.Os

1 Introduction

Nonlinear effects in plasmas involving multiple laser beams has been a subject attracting increasing attention in recent years. A few novel features have been found in various interaction configurations. These include the degenerate four wave mixing and phase-conjugating reflection [1], the superradiant amplification of an ultrashort laser pulse by a counter-propagating long pulse [3, 4], and electromagnetically induced guiding of counter-propagating laser pulses in a plasma [5], energy exchange of two intersecting laser beams in a streaming plasma [6, 7], braiding and hosing of two co-propagating beams [8, 9], etc. The interactions of two laser pulses in plasmas also finds applications in particle acceleration through the plasma beat-wave excitation [10], wake-field excitation of pulse trains [11], laser injection of electrons [12], colliding beam acceleration [13], crossed-modulated laser wake-fields [14], and stochastic heating and acceleration [15], etc.

✉ Fax: +86-10/8264-9531, E-mail: zmsheng@aphy.iphy.ac.cn

Recently, it has been shown that when two laser beams intersect at an overdense plasma surface, a grating-like electron density modulation is induced [16]. In the case of a single laser pulse interacting with a solid target, it has been shown that the incident and specularly reflected electromagnetic waves can also drive such a density modulation [17]. The oscillating component of the density modulation can serve as a moving mirror, which can efficiently convert the incident pulse into its high-harmonics, as shown theoretically and by simulations [18–20], and demonstrated experimentally [21–25]. Moreover, the slowly varying density modulation can act as a diffraction grating back-reflecting the incident pulse [17]. It should be noted that laser-induced gratings in various optical media have been studied extensively before [26]. Recently, laser-induced gratings have found new applications, such as the fabrication of periodic lateral nanostructures on semiconductor surfaces, laser surface modification, ultrafast optical switching, and laser-induced grating spectroscopy, etc. [27–30]. In underdense plasma, the bulk density modulations may find applications in the phase-matched relativistic harmonic generation [31], backward-wave oscillators [32], and the ion-ripple lasers [33, 34], where the latter may be used to generate X/γ-ray radiation. By use of refractive index gratings induced by counter-propagating intense laser pulses in a gas jet, quasi-phase-matched high-harmonic generation has been suggested [35, 36]. Obviously, an investigation of the electron and ion density gratings induced by two laser pulses in underdense plasma is necessary for some applications mentioned above.

This paper studies the formation of deep electron and ion density gratings in underdense plasma ($n_0/n_c \sim 0.01 - 0.5$) by use of two short counter-propagating/intersecting laser pulses at moderate intensities. In this case, one obtains bulk density gratings rather than surface gratings as in laser interaction with overdense plasma [16, 17]. Bulk plasma density gratings induced by infinite plane electromagnetic waves have been analyzed even earlier by M. Botton and A. Ron [32], where a stationary solution of the density modulation is given by assuming quasi-charge-neutrality in the interaction. The ion dynamics has been neglected, as well as in surface density grating formation [16, 17], where the electron density modulation is determined by assuming that the electrostatic force on the electrons is compensated by the ponderomotive force. Here, without these assumptions, the electron and ion dynam-

ics during the buildup of the density gratings are studied analytically and by particle-in-cell simulations. It was found that ion motion has important effects in the formation of the density gratings after the laser pulse interaction, even though the intensities of the ultrashort pump laser pulses are just around $10^{16}\,\mathrm{W\,cm^{-2}}$. Significant ion motion occurs in a time scale of $(M/m)^{1/2}(I_{18}\lambda^2)^{-1/2}\omega_0^{-1}$, which is around a few tens of laser cycles, $2\pi/\omega_0$, for the ion-electron mass ratio $M/m = 1800$ and laser intensity of $10^{16}\,\mathrm{W\,cm^{-2}}$. Here the laser intensity multiplied by the wavelength squared is normalized by $10^{18}\,\mathrm{W\,cm^{-2}\,\mu m^2}$.

In Sect. 2, the problem is studied analytically. Solutions of electron and ion density gratings at the linear stage will be given. A stationary solution is derived under the quasi-charge-neutrality condition, which is used to compare with the particle-in-cell (PIC) simulations. Section 3 presents the PIC simulations of the density grating formation for different parameters of the laser pulses and plasma. In Sect. 4 examples of the scattering of signal pulses by the preformed density gratings are shown. Emission of high-frequency radiation is observed. A summary is given in Sect. 5 with a discussion on the potential application of such density gratings to the ion-ripple laser.

2 Formulations of the problem

For simplicity, assume that two plane laser pulses counter-propagate along the x-axis. Since the focus of interest is in the induced plasma density modulation, the evolution of the laser pulses can be neglected for simplicity. As a result, the density modulation is governed by the following set of equations:

$$\partial p_{\mathrm{e},x}/\partial t = c\partial(\varphi - \bar{\gamma})/\partial x, \tag{1}$$

$$\partial n_\mathrm{e}/\partial t + c\partial(n_\mathrm{e} v_{\mathrm{e},x})/\partial x = 0, \tag{2}$$

$$\partial p_{\mathrm{i},x}/\partial t = -c(m/M)\partial\varphi/\partial x, \tag{3}$$

$$\partial n_\mathrm{i}/\partial t + c\partial(n_\mathrm{i} v_{\mathrm{i},x})/\partial x = 0, \tag{4}$$

$$\partial^2\varphi/\partial x^2 = (\omega_\mathrm{p}^2/c^2)(n_\mathrm{e} - n_\mathrm{i}), \tag{5}$$

where n_e and n_i are the electron and ion densities normalized by the unperturbed density n_0, respectively, φ is the scalar potential normalized by mc^2/e, $v_{\mathrm{e},x}$ and $v_{\mathrm{i},x}$ are the x-components of the electron and ion velocities normalized to the vacuum speed of light c, $p_{\mathrm{e},x}$ and $p_{\mathrm{i},x}$ are the x-components of the electron and ion momenta normalized by mc and Mc, respectively. Here m and M are the rest masses of electron and ion, respectively. Also, $\omega_\mathrm{p}^2 = 4\pi n_0 e^2/m$ is the electron plasma frequency. The simplified equations of motion (1) and (3) have been used following the derivation given in [37, 38]. For laser pulses at intensities well below the relativistic threshold of about $10^{18}\,\mathrm{W/cm^2}$, the relativistic factor can be written approximately as $\bar{\gamma} = 1 + \frac{1}{4}[a_1^2 + a_2^2 + 2a_1a_2\cos(2kx)]$, where $k = k_0(1 - n_0/n_c)^{1/2}$ is the laser wave vector in plasma, with $k_0 = \omega_0/c$ is the laser wave vector in vacuum. As a result, the normalized ponderomotive force is $F/(mc^2k_0) = -(c/\omega_0)(\partial\bar{\gamma}/\partial x) = (kc/\omega_0)a_1a_2\sin(2kx)$, if ignoring the finite pulse profile. Note that the ponderomotive force on ions in (3) is also neglected, which is smaller than the electrostatic field by the order of $O(m/M)$.

At the very beginning of the interaction of an ultrashort laser pulse with plasma, one can ignore the ion motion and assume a weak density perturbation of electrons. Letting $\delta n_\mathrm{e} = n_\mathrm{e} - 1$, obtains

$$\frac{\partial^2\delta n_\mathrm{e}}{\partial t^2} + \omega_\mathrm{p}^2\delta n_\mathrm{e} = c^2\frac{\partial^2}{\partial x^2}\bar{\gamma}\,. \tag{6}$$

Assuming that there is no density perturbation at the beginning: $\delta n_\mathrm{e}|_{t=0} = 0$ and $\partial\delta n_\mathrm{e}/\partial t|_{t=0} = 0$, obtains

$$\delta n_\mathrm{e} = -(2k^2c^2/\omega_\mathrm{p}^2)a_1a_2\cos(2kx)[1 - \cos(\omega_\mathrm{p}t)]\,, \tag{7}$$

and $\varphi = -(\omega_\mathrm{p}^2/4k^2c^2)\delta n_\mathrm{e}$. This approximation breaks down when $\delta n_\mathrm{e} \sim 1$ or $t > (2k^2c^2a_1a_2)^{-1/2}$. For $a_1 = a_2 = 0.1$, the time scale is about 1 laser cycles. Within this limitation, substituting φ and $\bar{\gamma}$ into (1), one obtains $p_{\mathrm{e},x} = (kc/\omega_\mathrm{p})a_1a_2\sin(\omega_\mathrm{p}t)\sin(2kx)$. In the generated electrostatic field, one finds that the ions move with $p_{\mathrm{i},x} = (kc/\omega_\mathrm{p})(m/M)$ $\times a_1a_2\sin(2kx)[\omega_\mathrm{p}t - \sin(\omega_\mathrm{p}t)]$ and the ion density perturbation changes like

$$\delta n_\mathrm{i} = -(k^2c^2/\omega_\mathrm{p}^2)(m/M)a_1a_2\cos(2kx) \times\left\{\omega_\mathrm{p}^2t^2 - 2[1 - \cos(\omega_\mathrm{p}t)]\right\}\,. \tag{8}$$

Comparing (7) and (8), it is clear that the modulation of the ion density is in phase with that of the electron density. They form a bulk grating-like structure with a wavelength of π/k. The time for building up significant ion density perturbations is $t \sim (M/m)^{1/2}(k^2c^2a_1a_2)^{-1/2}$, which scales like $(M/m)^{1/2}$. For $a_1 = a_2 = 0.1$ and $M/m = 1836$, it is within a time less than 100 laser cycles. Thus, the evolution of both the electron and ion density perturbations enters the nonlinear stage very quickly, and one has to resort to numerical simulations to obtain a complete picture about the grating-like density modulation.

For infinite plane waves, the stationary solution can be found. For this, one needs to add a thermal pressure term on the right-hand-sides of (1) and (3) with $-\partial P_{eT}/\partial x/(n_\mathrm{e}mc)$ and $-\partial P_{iT}/\partial x/(n_\mathrm{i}Mc)$, respectively. For a stationary solution, one has $\partial p_{\mathrm{e},x}/\partial t = 0$ and $\partial p_{\mathrm{i},x}/\partial t = 0$ on the left-hand-sides of (1) and (3), respectively. Meanwhile, there should be quasi-charge-neutrality for a long time, i.e, $Zn_\mathrm{i} \approx n_\mathrm{e}$. Assuming it is an isothermal process [39], one finds $\varphi = (\bar{\gamma} - 1)\varepsilon/(1 + \varepsilon)$ and $Zn_\mathrm{i} = n_\mathrm{e} = n_s\exp[-\mu\cos(2kx)]$ with $\mu = a_1a_2/[2\varepsilon_\mathrm{e}(1 + \varepsilon)]$, $\varepsilon = T_\mathrm{i}/ZT_\mathrm{e}$, $\varepsilon_\mathrm{e} = k_BT_\mathrm{e}/mc^2$, Z is the ion charge number, T_e and T_i are the electron and ion thermal temperatures, respectively, and n_s a constant needing determination. This density profile is quite similar to that obtained by Botton and Ron [32]. Now, from the Poisson's equation (5), one can find that the quasi-charge-neutrality is satisfied if $(k^2c^2/\omega_\mathrm{p}^2)a_1a_2\varepsilon \ll 1$. After normalization with the help of particle number conservation, one finds $n_s = 1/I_0(\mu)$ with I_0 the modified zero-order Bessel function. Using $I_0(\mu) \approx (2\pi\mu)^{-1/2}\exp(\mu)$ for $\mu \gg 1$, one obtains

$$Zn_\mathrm{i} \approx n_\mathrm{e} \approx (2\pi\mu)^{1/2}\exp\{-\mu[1 + \cos(2kx)]\} = (2\pi\mu)^{1/2}\exp[-2\mu\cos^2(kx)]\,, \tag{9}$$

which are normalized by the unperturbed density, n_0. This relation shows that the maximum plasma density is $n_{\max} =$

$\sqrt{2\pi\mu}$ and the width of the density peak around $2kx = (2N+1)\pi$ is $k\Delta x = 1/\sqrt{2\mu}$. Note that they are associated only with the combined variable μ, a quantity depending upon the laser amplitudes and the electron and ion temperatures. For example, if $a_1 = a_2 = 0.1$, $T_e = 10$ eV, and $T_i = 1$ eV, one obtains $n_{max} = 38.2n_0$. If taking $T_e = 100$ eV accounting for electron heating by the induced electrostatic field, one obtains $n_{max} = 12.6$. However, these maximum densities prove to be overestimated when compared with the simulation results given below.

3 Particle-in-Cell simulations

Since the interaction of crossing laser pulses with plasma involves deep plasma density modulations even if the intensities of the laser pulses are very low, such as 10^{15} W/cm^2, PIC simulations are used to study the buildup process of the plasma density gratings. For simplicity, simulations with a one-dimensional code are conducted. The simulation box has a dimension of 100λ with λ the laser wavelength in vacuum. A homogeneous plasma is located in the central region of the simulation box as shown in Fig. 1a. Two laser pulses with the same frequency ω_0 are launched from the two boundaries of the simulation box. They have the profiles $a_1 = a_{10}\sin^2(\pi t/t_L)$ and $a_2 = a_{20}\sin^2(\pi t/t_L)$ with $0 \le t \le t_L$ for the vector potential. Figure 1b shows the interaction geometry of two counter-propagating pulses in the simulation box, where $a_{10} = a_{20} = 0.1$ and $t_L = 60\tau$ for the laser pulses, and $n_0/n_c = 0.3$ for the plasma density. Here $\tau = 2\pi/\omega_0$ is the period of a laser cycle. The initial electron and ion temperatures are $T_e = 10$ eV and $T_i = 1$ eV, respectively. The mass ratio of ions to electrons is taken to be $M/m = 1836$ and the ion charge number to be $Z = 1$ in the simulations.

Figure 2 illustrates the buildup process of electron and ion density gratings for the laser and plasma parameters given in Fig. 1. Note that density peaks up to 4.6 times of the initial plasma density are produced both for electrons (Fig. 2a) and ions (Fig. 2b) at $t = 250\tau$, even though it is still much less than

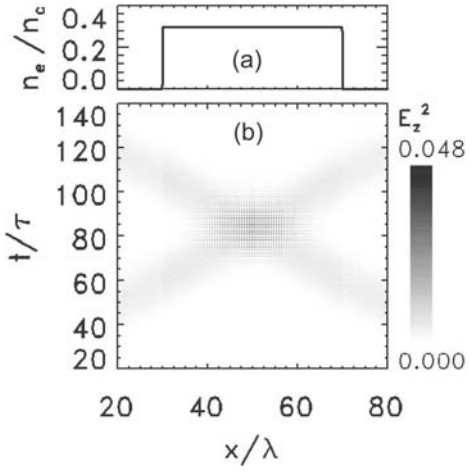

FIGURE 1 (a) This shows the initial plasma density distribution used in the simulations, where the peak density is $n_0/n_c = 0.3$; (b) shows the propagation of two counter-propagating pulses (called pump pulses) in the simulation box, where the two pulses are identical with a peak amplitude $a_{10} = a_{20} = 0.1$ and a duration $t_L = 60\tau$, where τ is the laser period of the pump pulses

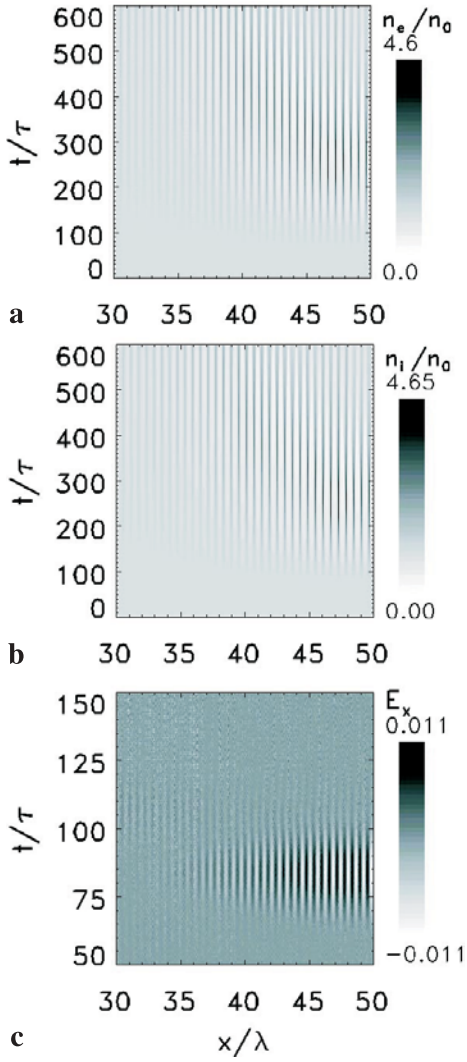

FIGURE 2 Evolution of the electron density, n_e/n_0 (**a**), the ion density, n_i/n_0 (**b**), and the induced electrostatic field, E_x (**c**) for plasma and laser pulse parameters as those given in Fig. 1. Note that there is symmetry around $x/\lambda = 50$ within $30 \le x/\lambda \le 70$

that estimated from the stationary solution given by (9). Electrostatic fields are found only during the intersecting stage of the two pulses as shown Fig. 2c. The maximum electrostatic field is found to be $E_{x,max}/(m\omega_0 c/e) = 0.01$ when the peaks of the two pulses are crossing each other at $t = 80\tau$. Its value is weakly dependent on the plasma density and is comparable to the ponderomotive force, i.e.,

$$\frac{E_{x,max}}{m\omega_o c/e} \approx \frac{c}{\omega_0}\frac{\partial\bar{\gamma}}{\partial x}|_{max} = \left(\frac{kc}{\omega_0}\right) a_{1m}a_{2m} = \frac{kc}{\omega_0}\frac{4}{(1+k/k_0)^2}a_{10}a_{20} \sim a_{10}a_{20}\,. \tag{10}$$

Here a_{1m} and a_{2m} are the peak amplitudes of the incident pulses in the plasma, which are related to their corresponding values in vacuum by $a_{1m} = [2/(1+k/k_0)]a_{10}$ and $a_{2m} = [2/(1+k/k_0)]a_{20}$, assuming $k/k_0 = (1-n_0/n_c)^{1/2} \sim 1$ still holds for underdense plasma, and $a_{10} \ll 1$ and $a_{20} \ll 1$ for low laser intensities. Quasi-charge-neutrality is realized quickly after the laser pulses propagate away, even though the grat-

ings are further deepened afterwards. This deepening process has been caused by the ion motion. During the laser crossing stage, electrons are pushed first by the ponderomotive force of the laser interference. As a result, electrostatic fields are induced. Ions are then pushed by the electrostatic fields before the quasi-charge-neutrality is realized. It is obvious that the formed density grating only occupies a region where the two pulses overlap. Figure 3 shows snapshots of the distributions of electron and ion momenta and the electron density. Around $t = 130\tau$, one finds full plasma neutralization, i.e., $n_e \approx n_i$ and $E_x \sim 0$. Therefore, ions already reach the maximum acceleration, even though the density grating is not very deep. The maximum velocity is about $0.00086c$, i.e.,

$$v_{i,\max} \sim kct_L(m/M)a_{10}a_{20}, \tag{11}$$

which basically corresponds to the calculation given in the last section. Later on, the electron density follows the ion density to maintain the quasi-charge-neutrality while the maximum ion density becomes higher and higher due to the ion motion, as shown in Fig. 3b. At later times, intercrossing of the neighboring ions set in around the density peaks, and the structures of ion density gratings begin to break. As a result, the density gratings of both electrons and ions decay with time afterwards.

A series of simulations were conducted to see the dependence of the grating formation on the initial plasma density, plasma temperature, laser pulse intensities, and their durations. First, when one changes the initial plasma density from $n_0/n_c = 0.01$ to 0.5, there is not much change in the formation of the density gratings. This agrees with the analysis given in the last section. For example, if the initial plasma density is set to be $n_0/n_c = 0.04$, this produced very similar results as for $n_0/n_c = 0.3$: the maximum electrostatic field is found to be about 0.01 at $t = 80\tau$ when the two pulse peaks cross each other, which follows (10); the peak ion velocity is found to be about $0.00085c$, around $t = 130\tau$, when the electrostatic field begins to disappear, which follows (11); the maximum density of the grating is about $4.2n_0$ around $t = 250\tau$.

In another case, the initial electron and ion temperatures were increased to $T_e = 100$ eV and $T_i = 10$ eV. In this case, it was found that the maximum density of the grating reduces to $2.7n_0$ around $t = 240\tau$. It is apparent that thermal pressure plays the role of reducing the density peaks, qualitatively in agreement with the theory in Sect. 2. Other results are similar to those given before. When increasing the ion mass to $M/m = 3672$ while keeping other parameters fixed, it is found that the maximum electrostatic field is found to be still 0.01

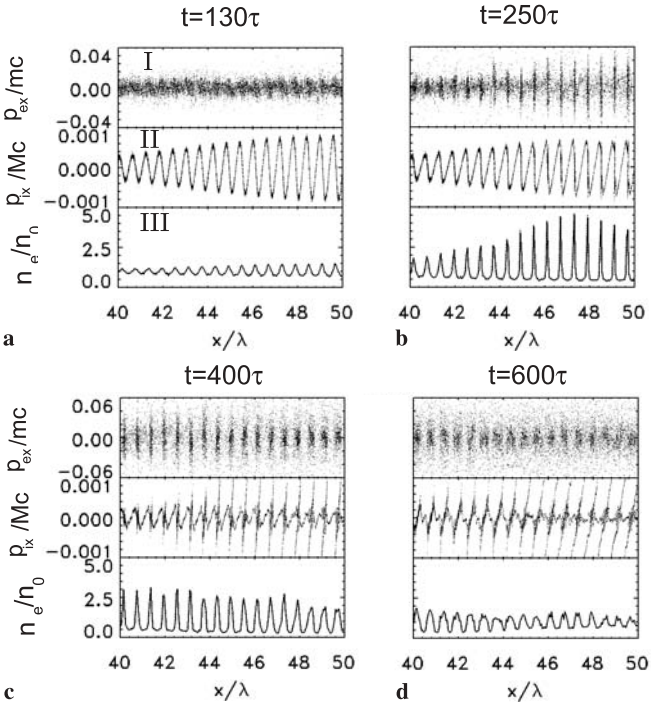

FIGURE 3 Snapshots of the longitudinal components of electron (frame I) and ion (frame II) momenta as well as the electron (in *solid lines*) and ion (in *dotted lines*) densities (frame III) at different times. The parameters for the plasma and laser pulses are the same as in Fig. 2. Note that one cannot distinguish the distribution of the ion density from that of the electron density plotted in this scale, indicating that a quasi-charge-neutrality state is achieved at these times

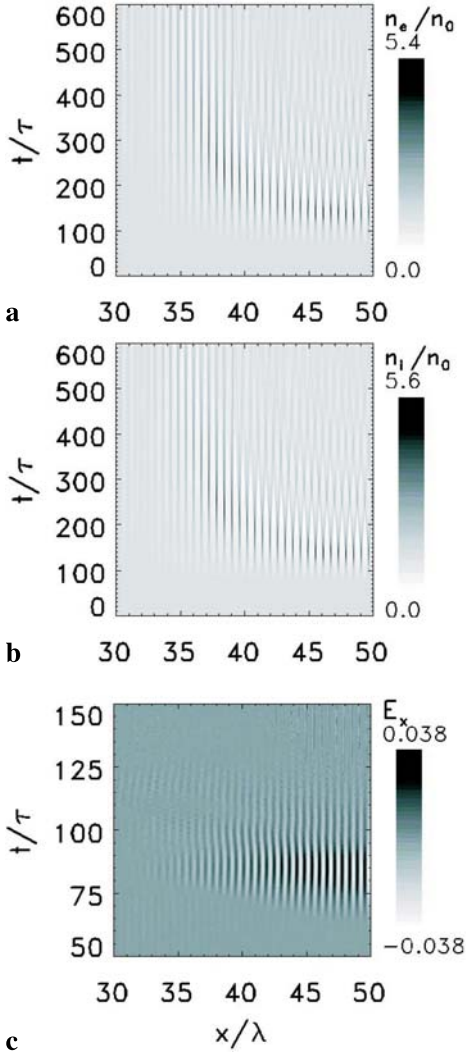

FIGURE 4 Evolution of the electron density, n_e/n_0 , (**a**) the ion density, n_i/n_0 , and (**b**) the induced electrostatic field, E_x (**c**) for plasma and laser pulse parameters as those given in Fig. 1, except for the pulse amplitudes $a_{10} = a_{20} = 0.2$. Note that there is symmetry around $x/\lambda = 50$ within $30 \le x/\lambda \le 70$

around $t = 80\tau$. The maximum ion velocity is about $0.00043c$ at $t = 120\tau$, in consistency with (11). As a result, it takes longer time to reach the maximum density. The maximum density of the grating reduces to $3.7n_0$ at $t = 400\tau$.

When increasing the pulse durations to $t_L = 90\tau$ while keeping the other parameters the same as in Fig. 2, it is found the maximum density of the grating increases to $5.3n_0$ at $t = 220\tau$. The maximum electrostatic field is found to be still 0.01 around $t = 100\tau$ when the peaks of the two pulses overlap each other. The maximum ion velocity is about $0.0013c$ at $t = 180\tau$, which is consistent with the fact that it is proportional to the pulse durations as shown by (11).

When increasing the pulse peak amplitudes to $a_{10} = a_{20} = 0.2$ while keeping other parameters fixed, the induced maximum electrostatic field is found to be about 0.038 around $t = 80\tau$. The maximum ion velocity is about $0.0032c$ at $t = 120\tau$. Again these are consistent with (10) and (11). The maximum density of the grating increases to $5.5n_0$ at $t = 130\tau$. Figure 4 shows the electron and ion densities, as well as the electrostatic field as a function of time and space. It demonstrates that the density grating decays with time more quickly than those obtained with lower light intensities. This is because of the high ion velocity so that the intercrossing of neighboring ions around the density peaks occurs more quickly. Figure 5 shows snapshots of the electron and ion momenta and the electron density. They are qualitatively similar to those given in Fig. 3. Note that when further increasing the pulse amplitudes, the peak amplitudes of the density gratings decrease. They also decay more quickly owing to the higher electron and ion velocities obtained during the interactions.

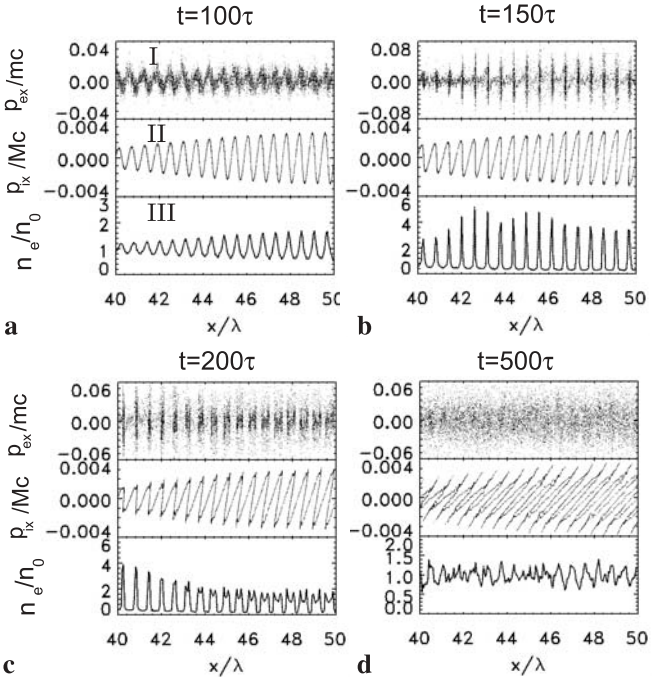

FIGURE 5 Snapshots of the longitudinal components of electron (frame I) and ion (frame II) momenta as well as the electron (in *solid lines*) and ion (in *dotted lines*) densities (frame III) at different times. The parameters for the plasma and laser pulses are the same as those in Fig. 4. Note that one cannot distinguish the distribution of the ion density from that of the electron density plotted in this scale, indicating that a quasi-charge-neutrality state is established at these times

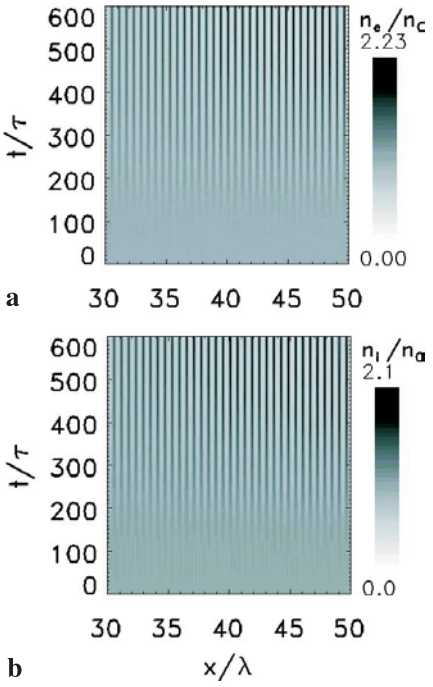

FIGURE 6 The evolution of the electron density, n_e/n_0 (**a**), and the ion density, n_i/n_0 (**b**) for similar plasma and laser pulse parameters as those given in Fig. 1, except for the pulse amplitude $a_{10} = a_{20} = 0.03$. Note that there is symmetry around $x/\lambda = 50$ within $30 \le x/\lambda \le 70$

Finally when reducing the pulse peak amplitudes to $a_{10} = a_{20} = 0.03$ while keeping other parameters unchanged from Fig. 2, it is found that a homogeneous density grating can be formed which subsists as long as a few picoseconds. The maximum density of the grating is about $2.2n_0$ at $t = 450\tau$ as shown in Fig. 6. The maximum ion velocity is about $0.0002c$ at $t = 400\tau$. Therefore, one can use laser pulses at intensities of 10^{15} W/cm^2 to generate long lasting density gratings for potential applications.

4 Examples of laser pulse scattering with density gratings and high-frequency radiation generation

Naturally it could be assumed that the bulk plasma density gratings as a kind of stratified index layers can scatter light as acoustic waves do in acousto-optic modulators [40]. To check this, first a density grating was produced such as given in Fig. 2, except for an initial plasma density of $n_0 = 0.5n_c$. The resulting density grating is similar to that given in Fig. 2; however, its maximum density exceeds the critical density associated with the pump pulses. Then a signal pulse with a duration of a few laser cycles and a peak amplitude of $a_{s0} = 0.01$ is launched into the density gratings from the left boundary. This signal pulse is incident with a polarization different from that of the pump pulses and with a central frequency $\omega_{s0} = 0.8\omega_0$. Figure 7a shows the backscattered light wave. Obviously it is composed of three parts. The first part is due to the left vacuum-plasma boundary, the second part is due to the electron density grating formed inside the plasma, and the third part is due to the right plasma-vacuum boundary. By taking Fourier transforms of these three parts, their frequency spectra are obtained, as shown in Fig. 7b. It was

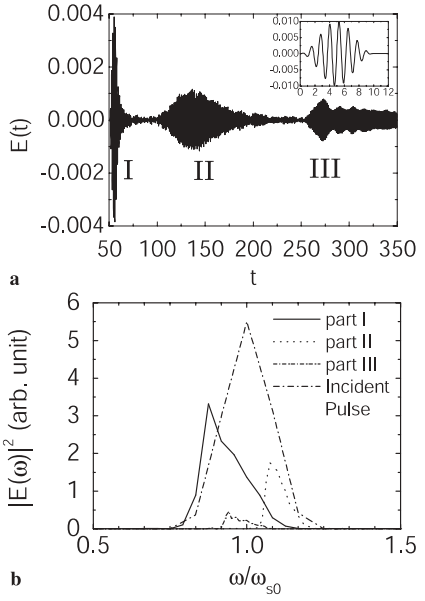

FIGURE 7 **a** Backscattered light of a short signal laser pulse (see *inserted frame*) from the density grating formed by the two pump laser pulses with the same parameters as those given in Fig. 1 and an initial electron density $n_0 = 0.5n_c$; The signal pulse is incident with a peak amplitude $a_{s0} = 0.01$ at the central frequency $\omega_{s0} = 0.8\omega_0$ and with a polarization different from the pump pulses. **b** Spectra of the different parts of the backscattered light

found that the frequency spectra of the parts I and III of the reflected wave are all slightly red-shifted, and the spectrum of part II appears slightly blue-shifted. These shifts may be attributed to the wide spectrum of the incident signal pulse of a few cycles, which extends down to the unperturbed electron plasma frequency $\omega_p = 0.707\omega_0$. Qualitatively, since the low frequency component of the signal pulse has a high reflectivity at the vacuum-plasma boundary, one observes the red-shifted parts I and III. Inside the density grating, the peak density is higher than the unperturbed density and the critical density associated with the central frequency of the signal pulse. Thus the high frequency component of the signal pulse can be reflected, leading to the blue-shifted part II. In addition, part III has a slightly higher frequency than part I. This is due to the presence of the density grating in the center, which tends to block the lower frequency component. Note that most of the signal pulse is still transmitted through the plasma slab with its central frequency unshifted.

If the amplitude of the signal pulse is increased, nonlinear scattering occurs, resulting in high-frequency radiation emission and breakdown of the bulk density grating. Figure 8 shows the spectra of the backscattered (a, and c) and transmitted (b, and d) light for $a_{s0} = 0.3$, $\omega_{s0} = 0.8\omega_0$, and $t_L = 60\tau$. When the unperturbed plasma density is relatively low such as $n_0 = 0.1n_c$, one observes emissions close to the harmonics of the pump pulse (at frequency ω_0) in the backscattered light. The spectrum of the transmitted light is still mainly peaked at the frequency of the incident signal pulse (see Fig. 8b). With the increase of the initial unperturbed plasma density, high-frequency components are observed both in the backscattered and transmitted light. Their frequencies are, however, shifted from the harmonic order of both the pump pulse and signal pulse (see Figs. 8c and d). Note that, at the same light intensity, the efficiency of high-frequency radiation generation is larger than that of relativistic laser harmonics in homogeneous underdense plasma [41], and is comparable to that of laser harmonics from solid surfaces [18–20].

In the next example, a plasma density grating with two pulses intersecting under 90 degrees was generated. In the two-dimensional(2D) PIC simulations, the two pump pulses are *s*-polarized (with electric component in z direction) and propagate along x and y directions, respectively. The pump pulses all have a peak amplitude of 0.2, a duration of 80τ, and are focused to 30λ in diameter. The initial plasma density is $n_0 = 0.5n_c$. Figure 9a shows the induced ion density grating at $t = 200\tau$. The electron density is almost the same as

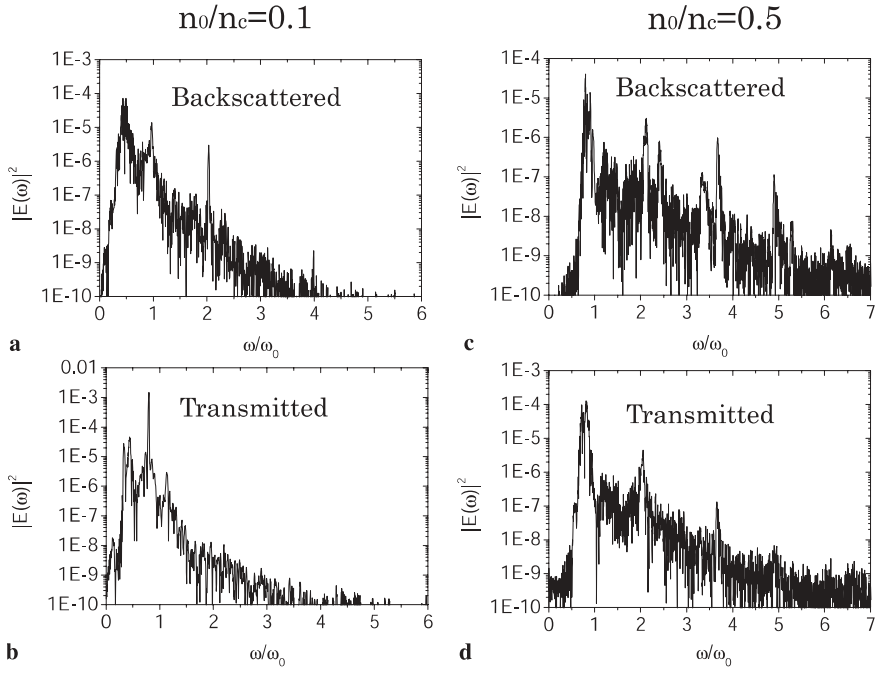

FIGURE 8 Spectra of backscattered and transmitted pulses in a density grating formed by two laser pulses with the same parameters as those given in Fig. 1. The signal pulse has $a_{s0} = 0.3$, $\omega_{s0} = 0.8\omega_0$, and $t_L = 60\tau$. Frames **a** and **b** show the backscattered and transmitted spectra, respectively, for the case with $n_0 = 0.1n_c$; frames **c** and **d** show the backscattered and transmitted spectra, respectively, for the case with $n_0 = 0.5n_c$

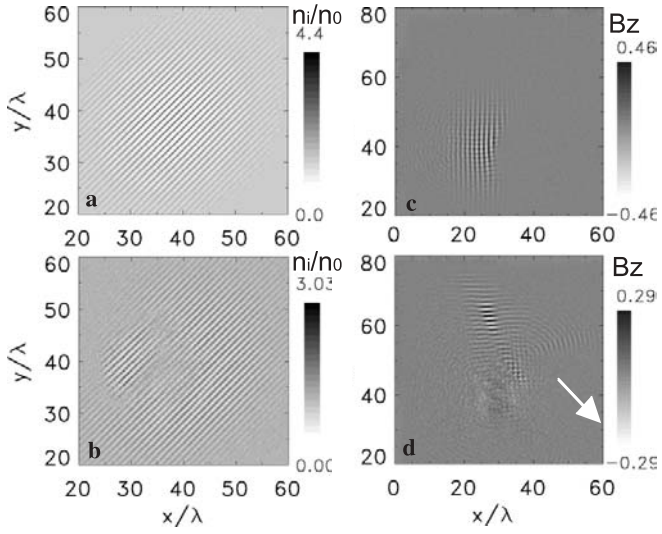

FIGURE 9 2D PIC simulations of the density grating induced by two s-polarized pump pulses, one along the x-direction and another along the y-direction. Both the pump pulses have a peak amplitude $a_{10} = a_{20} = 0.2$ and a duration of 80τ, and are focused to 30λ in diameter. The initial plasma density is $n_0 = 0.5n_c$. The signal pulse is incident with p-polarization along the x-axis, with a delay of 150τ relative to the pump pulses, and with a peak amplitude $a_{s0} = 0.3$, and is focused diameter of 20λ. **a** Ion density at 200τ; **b** Ion density at 300τ; **c** Signal pulse at 200τ; **d** Signal pulse at 240τ. The *arrow* in frame (**d**) shows the propagation direction of the emission near the second harmonic

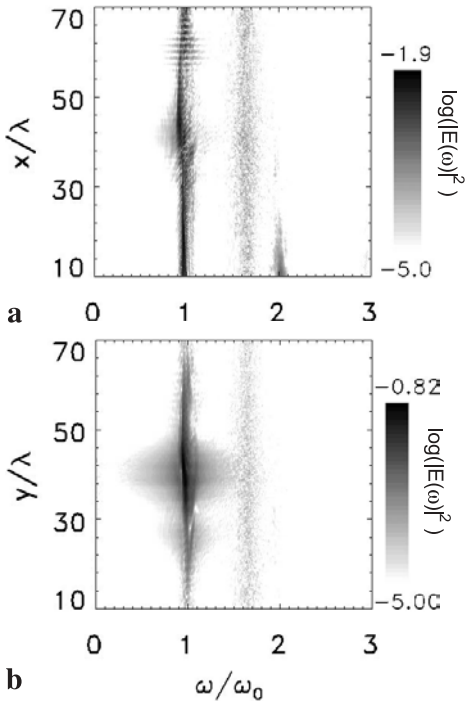

FIGURE 10 Spectra ($|E(\omega)|^2$ in logarithmic scale) of the transmitted light through the right x-boundary (**a**) and scattered light through the top y-boundary (**b**) as obtained in a 2D PIC simulation for laser and plasma parameters as those given in Fig. 9

the ion density at this time. A signal pulse is launched along the x-direction, which has a time delay of 150τ relative to the pump pulses. The signal pulse is p-polarized with the same central frequency as the pump pulses $\omega_{s0} = \omega_0$ and has a duration of about 30τ, a peak amplitude of 0.3, and a focused diameter of 20λ. Figure 9b shows the ion density after interaction, which is found to be deformed after the interaction. Figure 9c displays a snapshot of the magnetic field, B_z, of the incident signal pulse interacting with the density grating at $t = 200\tau$. This B_z field allows us to distinguish the signal pulse from the pump pulses. Figure 9d shows the distribution of the magnetic field component, B_z, of the signal pulse after interaction with the density gratings at $t = 240\tau$. It is found that a significant part of the signal pulse is scattered along the y-direction. A small amount of energy is still transmitted through the density grating even if the density peak in the grating is twice the critical density. From the Fourier transforms of the scattered and transmitted parts of the pulse, their frequency spectra are obtain as shown in Fig. 10. Here Fig. 10a shows the spectrum of the scattered wave through the top y-boundary in the simulation box and Fig. 10b the spectrum of the transmitted wave through the right x-boundary. It appears that after the interaction, there is a new frequency around $1.7\omega_0$ both in the scattered and transmitted light. Moreover, there is one emission near the second harmonic through the low right x-boundary, which has the same polarization as the signal pulse. This can be seen also in Fig. 9d. Qualitatively, similar features of the spectra for the scattered and transmitted light are observed as in 1D PIC case.

Up to now, however, the physical origins of the high-frequency emissions are still not clear. They are possibly related to the electron oscillation inside the bulk gratings driven by the signal pulse. There may also be some instability of the density grating under the signal pulse interaction. In a few other simulations, it is found that the spectra are related with the duration and intensity of the signal pulse. An identification of the physical mechanism of the emission is still quested.

5 Summary and discussions

The generation of deep plasma density gratings caused by two intersecting laser pulses at moderate intensities has been studied. It is produced through the interference of the two pulses which results in an intensity interference pattern. Since the distance between the intensity peaks can be less than a laser wavelength, a huge ponderomotive force is produced which drives electrons out of the high-intensity regions. As a result, electrostatic fields are induced. The maximum electrostatic field is found when the pump pulse peaks overlap, which depends mainly on the peak amplitudes of the pulses and more weakly on the initial plasma density. The ions build up velocities in the induced electrostatic field before the quasi-charge-neutrality is established in a time proportional to the pulse duration. Later on, electrons move and follow ions in a way so as to maintain the quasi-charge-neutrality. The maximum densities of electrons and ions in the formed grating are reached just before the on-set of the intercrossing of neighboring ions near the density peaks. Afterwards, with the intercrossing of neighboring ions, the density gratings decay with time. It was found that the maximum densities of electrons and ions depend on the pulse amplitudes and plasma temperatures. The analytic solutions agree qualitatively with the particle-in-cell simulations, even though the quasi-stationary solution (9) usually overestimates the maximum densities of

the induced gratings. If one uses pulses at a low intensity, such as a few 10^{15} W/cm^2, and a few hundred femtoseconds, the produced density gratings can last as long as a few tens of picoseconds.

When a signal pulse propagates in such a density gratings, it is found that the pulse can still be partially transmitted even if the peak density of the density grating exceeds the critical density. The pulse is also strongly scattered by the density grating. In addition to the radiation at the frequency of the original signal pulse, radiations also exist at higher frequencies both in the scattered and transmitted waves. Their physical origin is not clear. They are possibly related to electron oscillations driven by the signal pulse in the density gratings.

A possible application of the produced density gratings is in the ion-ripple laser as proposed by Chen and Dawson [34]. It is supposed to be able to generate radiation at the resonant frequency $\sim 2\gamma_b^2 K_g c \cos\theta$, where γ_b is the relativistic factor of the incident electron beam, K_g is the wave number of the density grating, θ is the incident angle of the electron beam against the grating vector. It is obvious that very high-frequency radiation in the hard X-ray regime at a few angstroms in wavelength can be generated with electron beams at a few tens of MeV if such density gratings discussed above are employed. Since the density modulation is nearly 100% in our case, it is expected that the growth rate and the efficiency can increase significantly as compared with the primary scheme of ion-ripple lasers by use of an acoustic grating. Moreover, harmonics of the above mentioned resonant frequency can be generated owing to the deep modulation in the density gratings, where the latter also contains harmonics at wave numbers NK_g. However, a theoretical analysis of this problem is still required, with plasma density gratings produced in such a way as discussed in this paper.

ACKNOWLEDGEMENTS We wish to thank Dr. X. Lu, Dr. J.A. Zheng, and many colleagues in the laboratory for some useful discussions on this work. This work has been supported in part by the National Natural Science Foundation of China (Grant Nos. 10105014, 19825110, 10075075), the Bairen Jihua Program of the Chinese Academy of Sciences, the National High-Tech ICF Committee in China, National Key Basic Research Special Foundation (NKBRSF) under Grant No. G1999075200, and the U.S. National Science Foundation.

NOTE ADDED IN PROOF Related works on the interaction of intersecting laser pulse in underdense plasma in the high-intensity regime can be found in recent publications: P. Zhang et al., Phys. Plasmas **10**, 2093 (2003) and Phys. Rev. Lett. (to be published).

REFERENCES

1 I. Nebenzahl, A. Ron, N. Rostoker: Phys. Rev. Lett. **60**, 1030 (1988)
2 J.X. Ma, R. Chen, Z. Xu, J. Op. Soc. Am. B **8**, 1442 (1991)
3 G. Shvets, N.J. Fisch, A. Pukhov, J. Meyer-ter-Vehn: Phys. Rev. Lett. **81**, 4879 (1998); Y. Ping, I. Geltner, N.J. Fisch, G. Shvets, S. Suckewer: Phys. Rev. E **62**, R4532 (2000)
4 V.M. Malkin, G. Shvets, N.J. Fisch: Phys. Plasmas **7**, 2232 (2000)
5 G. Shvets, A. Pukhov: Phys. Rev. E. **59**, 1033 (1999)
6 C.J. McKinstrie, J.S. Li, R.E. Giacone, H.X. Vu: Phys. Plasmas **3** 2686 (1996); ibid. **5**, 1142 (1998)
7 W.L. Kruer, S.C. Wilks, B.B. Afeyan, R.K. Kirkwood: Phys. Plasmas **3**, 382 (1996); V.V. Eliseev, W. Rozmus, V.T. Tikhonchuk, C.E. Capjack: ibid. **3**, 2215 (1996); H.A. Rose, S. Ghosal, ibid. **5**, 1461 (1998); C. Labaune, H.A. Baldis, B. Cohen, W. Rozmus, S. Depierreux, E. Schifano, B.S. Bauer, A. Michard: ibid. **6**, 2048 (1999); K.B. Wharton, R.K. Kirkwood, S.H. Glenzer, K.G. Estabrook, B.B. Afeyan, B.I. Cohen, J.D. Moody, B.J. MacGowan, C. Joshi: ibid. **6**, 2144 (1999)
8 C. Ren, R.G. Hemker, R.A. Fonseca, B.J. Duda, W.B. Mori: Phys. Rev. Lett. **85**, 2124 (2000); Phys. Rev. E **64**, 067401 (2001); Phys. Plasmas **9**, 2354 (2002)
9 Q.L. Dong, Z.-M. Sheng, J. Zhang: Phys. Rev. E **66**, 027402 (2002)
10 M.N. Rosenbluth, C.S. Liu: Phys. Rev. Lett. **29**, 701 (1972); T. Tajima, J.M. Dawson: Phys. Rev. Lett. **43**, 267 (1979); R.J. Noble: Phys. Rev. A **32**, 460 (1985)
11 D. Umstadter, E. Esarey, J. Kim: Phys. Rev. Lett. **72**, 1224 (1994); V.I. Berezhziani, I.G. Murusidze, Physica Scripta **45**, 87 (1992); S. Dalla, M. Lontano: Phys. Rev. E **49**, R1819 (1994); G. Bonnaud, D. Teychenne, J.L. Bobin: Phys. Rev. E **50**, R36 (1994)
12 D. Umstadter J.K. Kim, E. Dodd: Phys. Rev. Lett. **76**, 2073 (1996); E. Esarey, R.F. Hubbard, W.P. Leemans, A. Ting, P. Sprangle: Phys. Rev. Lett. **79**, 2682 (1997)
13 G. Shvets, N.J. Fisch, A. Pukhov, J. Meyer-ter-Vehn: Phys. Rev. E **60**, 2218 (1999)
14 Z.-M. Sheng, K. Mima, Y. Sentoku, K. Nishihara, J. Zhang: Phys. Plasmas **9**, 3147 (2002)
15 Z.-M. Sheng, K. Mima, Y. Sentoku, M.S. Jovanovic, T. Taguchi, J. Zhang, J. Meyer-ter-Vehn: Phys. Rev. Lett. **88**, 055004 (2002)
16 L. Plaja, L. Roso: Phys. Rev. E **56**, 7142 (1997)
17 A.A. Andreev, K.Yu. Platonov, R.R.E. Salomaa: Phys. Plasmas **9**, 581 (2002)
18 R. Lichters, J. Meyer-ter-Vehn, A. Pukhov: Phys. Plasmas **3**, 3425 (1996)
19 P. Gibbon: Phys. Rev. Lett. **76**, 50 (1996)
20 D. von der Linde, K. Rzàzewski: Appl. Phys. B **63**, 499 (1996)
21 S. Kohlweyer, G.D. Tsakiris, C.G. Wahlström, C. Tillman, I. Mercer: Opt. Commum. **177**, 431 (1995)
22 P.A. Norreys, M. Zepf, S. Moustaizis, A.P. Fews, J. Zhang, P. Lee, M. Bakarezos, C.N. Danson, A. Dyson, P. Gibbon, P. Loukakos, D. Neely, F.N. Walsh, J.S. Wark, A.E. Dangor: Phys. Rev. Lett. **76**, 1832 (1996)
23 M. Zepf, G.D. Tsakiris, G. Pretzler, I. Watts, D.M. Chambers, P.A. Norreys, U. Andiel, A.E. Dangor, K. Eidmann, C. Gahn, A. Machacek, J.S. Wark, K. Witte: Phys. Rev. E **58**, R5253 (1998)
24 D. von der Linde: Appl. Phys. B **68**, 315 (1999); A. Tarasevitch, A. Orisch, D. von der Linde, P. Balcou, G. Rey, J.-P. Chambaret, U. Teubner, D. Klöpfel, W. Theobald: Phys. Rev. A **62**, 023816 (2000)
25 U. Teubner, G. Pretzler, T. Schlegel, K. Eidmann, E. Förster, K. Witte: Phys. Rev. A **67**, 013816 (2003)
26 H. Kalt, V.G. Lyssenko, R. Renner, C. Klingshirn: J. Opt. Soc. Am. B **7**, 1188 (1985), and refs. therein
27 T.H. Metzger, K. Haj-Yahya, J. Peisi, M. Wendel, H. Lorenz, J.P. Kotthaus: J. Appl. Phys. **81**, 1212 (1997)
28 D. Walgraef, N.M. Ghoniem: J. Comp.-Aided Mat. Des. **6**, 323 (1999)
29 T. Schneider, D. Wolfframm, R. Mitzner, J. Reif: Appl. Phys. B **68**, 749 (1999)
30 D.E. Govoni, J.A. Booze, A. Sinha, F.F. Crim: Chem. Phys. Lett. **216**, 525 (1993); J.A. Booze, D.E. Govoni, F.F. Crim: J. Chem. Phys. **103**, 10484 (1995); A.G. Gorshunov, V. N. Grigor'ev, V.I. Grinev, K.L. Litvinenko, V.G. Lysenko, JETP **82**, 356 (1996); D.N. Kozlov, R. Bombach, B. Hemmrling, W. Hubschmid: Opt. Lett. **22**, 46 (1997)
31 J.M. Rax, N.J. Fisch: Phys. Rev. Lett. **69**, 772 (1992); IEEE Trans. Plasma Sci. **21**, 105 (1993)
32 M. Botton, A. Ron: Phys. Rev. Lett. **66**, 2468 (1991)
33 H. Kupershmidt, A. Ron: Appl. Phys. Lett. **63**, 1733 (1993)
34 K.R. Chen, J.M. Dawson: Phys. Rev. Lett. **68**, 29 (1992), K.R. Chen, J.M. Dawson: Phys. Rev. A **65**, 4077 (1992)
35 S.L. Voronov, I. Kohl, J.B. Madsen, J. Simmons, N. Terry, J. Titensor, Q. Wang, J. Peatross: Phys. Rev. Lett. **87**, 133902 (2001)
36 K. Mima: private communications (2003)
37 P. Sprangle, E. Esarey, J. Krall, G. Joyce: Phys. Rev. Lett. **69**, 2200 (1992)
38 Z.-M. Sheng, J. Meyer-ter-Vehn, A. Pukhov: Phys. Plasmas **5**, 3764 (1998)
39 If assuming that it is an adiabatic process, then one obtains $n_e \approx Zn_i \approx (2\mu/3)^{1/2} n_0 [C - \cos(2kx)]^{1/2}$ in the quasi-neutrality approximation. Thus there is $C \geq 1$. In this case, one finds that the particle number conservation cannot be satisfied
40 H.A. Haus: *Waves and Fields in Optoelectronics* (Prentice-Hall, Inc., Englewood Cliffs, New Jersey 1984) Chapt. 9
41 E. Esarey, A. Ting, P. Sprangle, D. Umstadter, X. Liu: IEEE Trans. Plasma Sci. **21**, 95 (1993); W.B. Mori, C.D. Decker, W.P. Leemann: ibid. **21**, 110 (1993); B. Shen, W. Yu, G. Zeng, Z. Xu: Phys. Plasmas **2**, 4631 (1995)